Supplemental Materials

Molecular Biology of the Cell

Ghosh et al.

SUPPLEMENTAL MATERIALS

Sec14-Nodulin Proteins Pattern Phosphoinositide Landmarks For Developmental Control of Membrane Morphogenesis

Ratna Ghosh[1‡], Marília K.F. de Campos[2‡], Jin Huang[1], Seong K. Huh[1], Adam Orlowski[3], Yuan Yang[4], Ashutosh Tripathi[1], Aaron Nile[1], Hsin-Chieh Lee[2], Marek Dynowski[5], Helen Schäfer[2], Tomasz Róg[3], Marta G. Lete[6], Hasna Ahyayauch[6,7], Alicia Alonso[6], Ilpo Vattulainen[3,8], Tatyana I. Igumenova[4], Gabriel Schaaf[2]*, and Vytas A. Bankaitis[1,4,9]

[1]Department of Molecular and Cellular Medicine, College of Medicine
Texas A&M Health Sciences Center
College Station, Texas 77843-1114, USA

[2]ZMBP, Plant Physiology, Universität Tübingen
72076 Tübingen, Germany

[3]Department of Physics
Tampere University of Technology
FI-33101 Tampere, Finland

[4]Department of Biochemistry & Biophysics
Texas A&M University
College Station, Texas 77843-2128

[5]ZDV, Universität Tübingen
72074 Tübingen, Germany

[6] Unidad de Biofísica (CSIC, UPV/EHU), Departamento de Bioquímica,
Universidad del País Vasco, Leioa, Spain

[7]Institut de Formation, aux Carrieres de Sante de Rabat (IFCSR)
Rabat, Morocco

[8]MEMPHYS – Center for Biomembrane Physics
University of Southern Denmark
DK-5230, Odense M, Denmark

[9]Department of Chemistry
Texas A&M University
College Station, Texas 77843-2128

SUPPLEMENTAL FIGURE LEGENDS

Supplemental Figure S1. Localization of Class 1-III nodulins in yeast. The indicated GFP-tagged **(A)** Class II and **(B)** Class III nodulins were expressed and localized in WT yeast cells. Images are representative of 130, 103, 103, 94, 126, 102 and 138 cells expressing AtSfh4, AtSfh5, AtSfh6, AtSfh8, AtSfh9, AtSfh13 and AtSfh14 nodulins, respectively. Cells expressing GFP-AtSfh6, -AtSfh9, -AtSfh13 and -AtSfh14 nodulins showed exclusive cytoplasmic localization for each of the corresponding chimeras, whereas the GFP-AtSfh4 and –AtSfh5 nodulins localized to the nucleus as evidenced by DAPI co-staining. GFP-AtSfh8 nodulin showed a dual PM and cytoplasmic localization as 67% of the cells showed both PM and cytoplasmic profiles for the GFP-chimera and 33% showed exclusively cytoplasmic profiles. (**C,D**) Localization of Class I nodulins is PtdIns(4,5)P_2-dependent. Confocal images of GFP-tagged AtSfh3, AtSfh7 and AtSfh10 nodulins expressed in yeast carrying: (**C**) four independent temperature sensitive alleles of the Mss4 PtdIns(4)P 5-OH kinase responsible for production of PtdIns(4,5)P_2, and **(D)** temperature sensitive alleles of the genes encoding each of the two essential yeast PtdIns-4-OH kinases (*pik1*^{ts} and *stt4*^{ts}) responsible for PtdIns(4)P production and of the potentiator of PtdIns 4-OH kinase activity Sec14 (*sec14*^{ts}) as indicated. Transformants of a *vps34Δ* strain lack the non-essential PtdIns 3-OH kinase required for production of both PtdIns(3)P and PtdIns(3,5)P_2. None of the lipid kinase defects of panel D affect PtdIns(4,5)P_2 levels under the conditions of these experiments, and inactivation of any one of these functions fails to release Class I nodulins from the PM. But, all Class I nodulins are released from the PM upon reduction of PtdIns(4,5)P_2 levels. All *ts* alleles have 22°C and 37°C as permissive and restrictive temperatures, respectively. Corresponding DIC and GFP confocal image panels are identified. Scale bars: 2 μm.

For panel (C), images are representative of an aggregate of 1284 and 1460 cells imaged at 22°C and 37°C, respectively, and 70-169 cells were scored for each nodulin at each temperature. In all cases, >96% of the cells imaged at 22°C showed PM localization of the GFP-nodulin reporter whereas, in all cases, >90% of the cells imaged at 37°C showed exclusively cytoplasmic localization for the indicated GFP-nodulin reporter. GFP-nodulin profiles were also imaged in WT yeast at 22°C (aggregate of 829 cells) and 37°C (aggregate of 292 cells). As expected, at both temperatures, >99% of the cells showed exclusively PM localization profiles. For panel (D), 32-302 cells were imaged for each mutant at each temperature. For each mutant and condition, >89% of the cells imaged showed exclusive PM localization for the indicated GFP-nodulin reporter.

Supplemental Figure S2. Localization of WT and mutant AtSfh1 nodulin domains in transiently expressing tobacco leaf epidermal cells and AtSFH1 nodulin-dependent PtdIns(4,5)P_2 homeostasis in Arabidopsis root hairs. *Nicotiana benthamiana* leaves transiently expressing mRFP-tagged WT nodulin and mutant versions with indicated single **(A)** and multiple **(B)** Lys to Ala substitutions were imaged by confocal scanning microscopy. A Bri1-GFP fusion was co-transfected as a plasma membrane marker. Merged and brightfield images are shown. Scale bars: 5 μm. **(C)** Proteins expressed in this experiment are stable as indicated by immunoblot analyses. **(D)** Loss of tip-directed PtdIns(4,5)P_2 gradients in Atsfh1$^{0/0}$ plants expressing Atsfh1 mutant transgenes. PtdIns(4,5)P_2 distribution was visualized as $PH_{PLC\delta1}$-YFP fluorescence in 3-day old *Atsfh1*$^{0/0}$ seedlings expressing: the *AtSFH1* (WT) transgene, the indicated transgenes with single K → A substitutions in the nodulin peptide that yield partially functional AtSfh1 proteins, or transgenes driving expression of the indicated multiply K → A substituted AtSfh1 proteins that

are biologically non-functional (bottom panel). The tip directed PtdIns(4,5)P_2 accumulation is highlighted by arrows. Scale bar: 10μm.

The relative intensities of $PH_{PLC\delta1}$-YFP fluorescence at the tip plasma membrane (PM) vs cortical PM were calculated using the Image J tool to measure line-scan intensities perpendicularly across tip and cortical membrane at three different positions for each TIFF image file by plot profiling. Background correction was applied to all the images before line scan. The maximum pixel intensities recorded across each set of line scans were averaged for tip PM to cortical PM. These values were used to generate tip PM/cortical PM fluorescence intensity ratios that were interpreted as semi-quantitative readouts for tip-directed PtdIns(4,5)P_2 gradients. In the WT case the tip PM/cortical PM intensity ratio was 4.2, a value in excellent agreement with our previous ratiometric imaging measurements that reported 3- to 4-fold PtdIns(4,5)P_2 enrichments in tip PM relative to cortical PM in growing root hairs (Vincent et al., 2005). AtSfh1-deficient root hairs reconstituted with the hypomorphic AtSfh1^{K5A} and AtSfh1^{K6A} proteins exhibited tip PM/cortical PM intensity ratios of 2.5 and 2.1, respectively. AtSfh1-deficient root hairs reconstituted with the functional null AtSfh1^{K3,5A}, AtSfh1^{K4,5A}, AtSfh1^{K3,4,5A}, and AtSfh1^{K1-7A} polypeptides exhibited tip PM/cortical PM intensity ratios of 1.2, 0.9, 0.7, and 0.5, respectively.

Supplemental Figure S3. High affinity of AtSfh1 nodulin for PtdIns(4,5)P_2 and gel filtration profiles of Class II nodulins. **(A)** Time course analysis of FM4-64 internalization in yeast. PMs of WT cells expressing GFP, GFP-AtSfh1 nodulin or GFP-AtSfh1^{K1-7A} nodulin were loaded with FM4-64 dye (10 μM) at 0°C, warmed to 30°C and imaged at each of the indicated time points. Scale bars: 5 μm. For the GFP and GFP-AtSfh1^{K1-7A} nodulin-expressing cells, 100-349 cells

were imaged and scored for each time point. At 2 min, 60% and 47% of the GFP cells and 53% and 43% of the GFP-AtSfh1^{K1-7A} cells showed both PM + endosome or only endosome staining, respectively. In both cases, 100% of the cells showed only endosomal staining at 7.5. min, both endosomal and vacuolar staining at 12 min, and exclusively vacuolar staining by 15 min. The kinetics of FM4-64 chase were delayed in GFP-AtSfh1-expressing cells. At 2 min, 87% and 13% of the cells showed both PM + endosome or only endosome staining, respectively, 81% of the cells still showed PM + endosome staining at 7.5 min. At 12 min, 90% of the cells showed label in PM, endosomes and vacuoles and >90% of cells still exhibited detectable PM pools of FM4-64 at 15, 30 and 60 min. **(B)** An mRFP tagged AtSfh1 nodulin remains on the plasma membrane in a yeast temperature sensitive PtdIns 4-P 5-OH kinase mutant (*mss4-102^{ts}*) at a semi-permissive temperature (26°C, left panel). By comparison, targeting of the tandemized PtdIns(4,5)P_2 biosensor GFP-2XPH$^{PLC\delta}$ to the PM was compromised at 26°C in the same *mss4-102^{ts}* strain (right panel). The pRS426-GFP-2XPH$^{PLC\delta}$ plasmid expressing the tandemized biosensor was obtained from Addgene (plasmid 36092). Scale bars: 5 μm. **(C)** Measurement of the binding of AtSfh1 nodulin C-terminal 12-mer peptide and the mutant peptides K_5A and $K_{3,5}A$ (peptide sequences at bottom) to small unilamellar vesicles (SUVs) containing 3 mol% PtdIns(4,5)P_2 by isothermal titration calorimetry. Top panel: heat exchange after the successive injections. Bottom panel: heat per mole of lipid as a function of lipid:peptide molar ratio. **(D)** Table showing thermodynamic parameters of binding of wild-type and mutant peptides to large unilamellar vesicles (LUVs). Data (average values ± S.D., n = 2-3) were obtained from experiments as the one shown in **C**. **(E)** Plot of association constants K_2 (data obtained from Table shown in **D**) of WT and mutant nodulin peptides binding to liposomes containing 3 mol% PtdIns(4,5)P_2. Unpaired t-test p value is shown (mutant compared to WT). **(F)** Gel filtration

profile for purified native AtSfh5 nodulin. **(G)** Gel filtration chromatogram for purified native AtSfh8 nodulin. Immunoblot profiles across the elution window are shown in the upper panels at top, and elution positions for the indicated standards are identified by arrows.

Supplemental Figure S4. Localization of AtSfh1nodulin proline substitution mutants in yeast deficient in defined lipid kinase activities. Confocal images of GFP-tagged AtSfh1 nodulin domains harboring the indicated single and double proline missense substitutions expressed in yeast carrying: **(A)** four independent temperature sensitive alleles of the Mss4 PtdIns(4)P 5-OH kinase responsible for production of PtdIns(4,5)P_2, and **(B)** temperature sensitive alleles of the genes encoding each of the two essential yeast PtdIns-4-OH kinases (*pik1*^{ts} and *stt4*^{ts}) responsible for PtdIns(4)P production and of the potentiator of PtdIns 4-OH kinase activity Sec14 (*sec14*^{ts}) as indicated. *vps34Δ* mutants lack the non-essential PtdIns 3-OH kinase required for production of both PtdIns(3)P and PtdIns(3,5)P_2. None of the lipid kinase defects of panel B affect PtdIns(4,5)P_2 levels under these experimental conditions, and inactivation of any one of these enzymes fails to release the mutant nodulins from the PM. But, both mutant Class I nodulins were released from the PM upon reduction in PtdIns(4,5)P_2 levels. All *ts* alleles have 22°C and 37°C as permissive and restrictive temperatures, respectively. DIC and GFP panels are labeled. Scale bars: 5 μm.

For panel (A), images are representative of an aggregate of 399 and 395 and 220 and 227 cells imaged for GFP-AtSfh1^{E485P} and GFP-AtSfh1^{E485P,Y474P} nodulins at 22°C and 37°C, respectively (41-155 cells were scored for each nodulin at each temperature). In both cases, >94% of the cells imaged at 22°C showed exclusively PM localization of the GFP-nodulin reporter whereas, in both cases, >93% of the cells imaged at 37°C showed exclusively

cytoplasmic localization for the indicated GFP-nodulin reporter. GFP-nodulin profiles were also imaged in WT yeast at 22°C (aggregate of 105 cells) and 37°C (aggregate of 143 cells). As expected, at both temperatures, >99% of the cells showed exclusively PM localization profiles.

For panel (B), 23-120 cells were imaged for each mutant at each temperature. For each mutant and condition, >93% of the cells imaged showed exclusive PM localization for the indicated GFP-nodulin reporter. GFP-nodulin profiles were also imaged in WT yeast at 22°C (aggregate of 81 cells) and 37°C (aggregate of 114 cells). As expected, at both temperatures, >99% of the cells showed exclusively PM localization profiles.

Figure S1

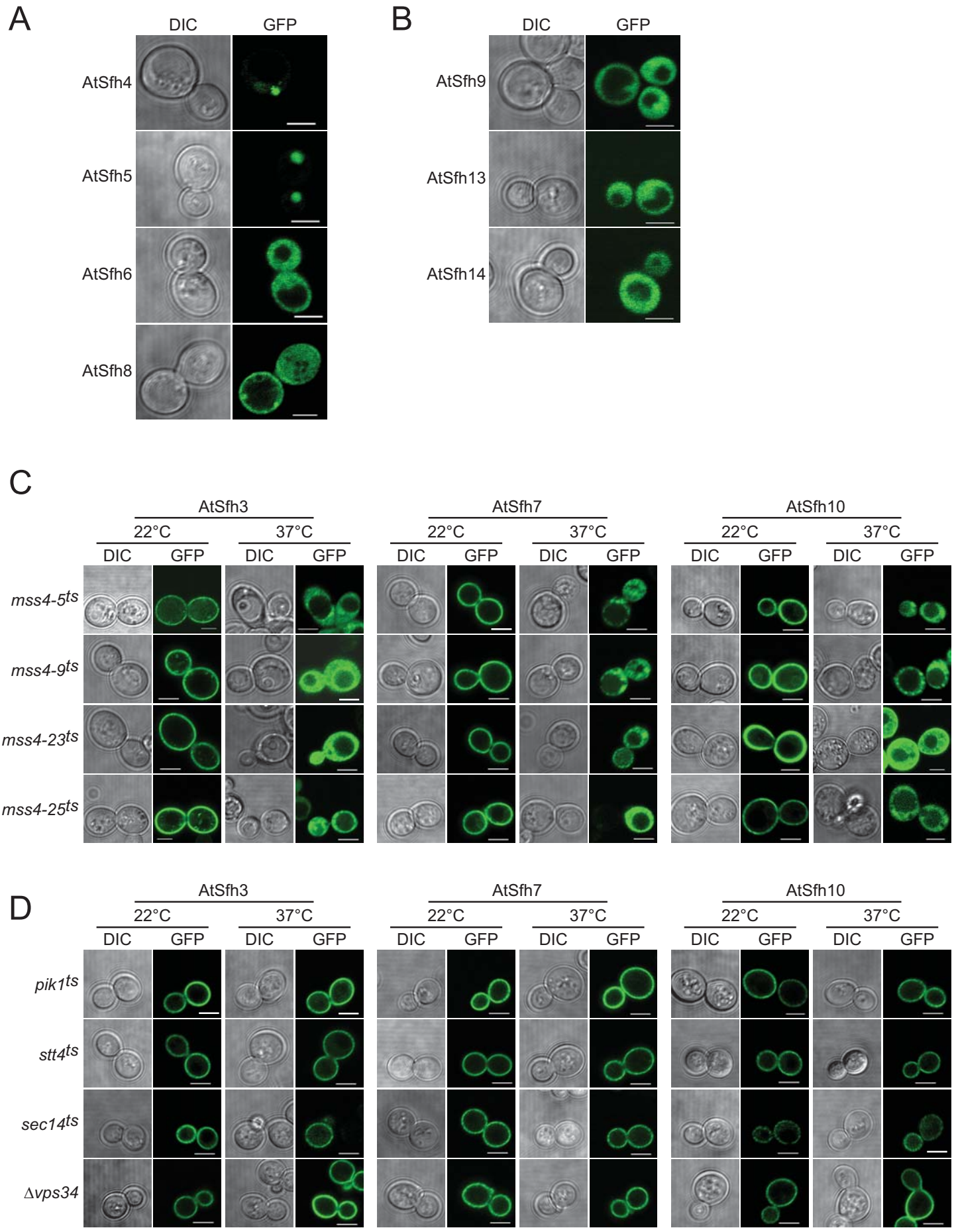
A
DIC
GFP
AtSfh4
AtSfh5
AtSfh6
AtSfh8
B
DIC
GFP
AtSfh9
AtSfh13
AtSfh14
C
AtSfh3
AtSfh7
AtSfh10
22°C
37°C
DIC
GFP
mss4-5ts
mss4-9ts
mss4-23ts
mss4-25ts
D
AtSfh3
AtSfh7
AtSfh10
22°C
37°C
DIC
GFP
pik1ts
stt4ts
sec14ts
Δvps34

Figure S2

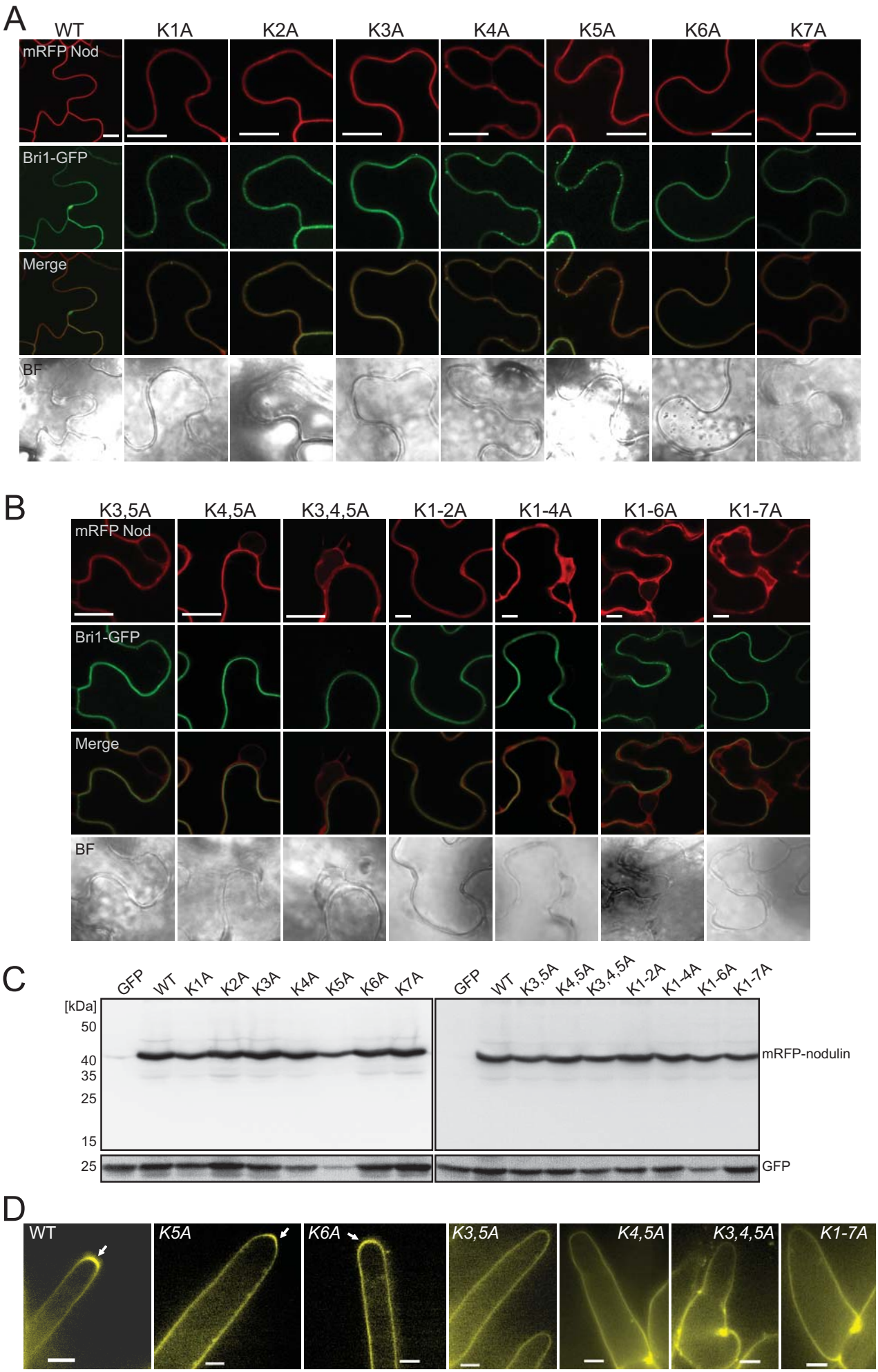
A
WT
K1A
K2A
K3A
K4A
K5A
K6A
K7A
mRFP Nod
Bri1-GFP
Merge
BF
B
K3,5A
K4,5A
K3,4,5A
K1-2A
K1-4A
K1-6A
K1-7A
mRFP Nod
Bri1-GFP
Merge
BF
C
GFP
WT
K1A
K2A
K3A
K4A
K5A
K6A
K7A
GFP
WT
K3,5A
K4,5A
K3,4,5A
K1-2A
K1-4A
K1-6A
K1-7A
[kDa]
50
40
35
25
15
25
mRFP-nodulin
GFP
D
WT
K5A
K6A
K3,5A
K4,5A
K3,4,5A
K1-7A

Figure S3

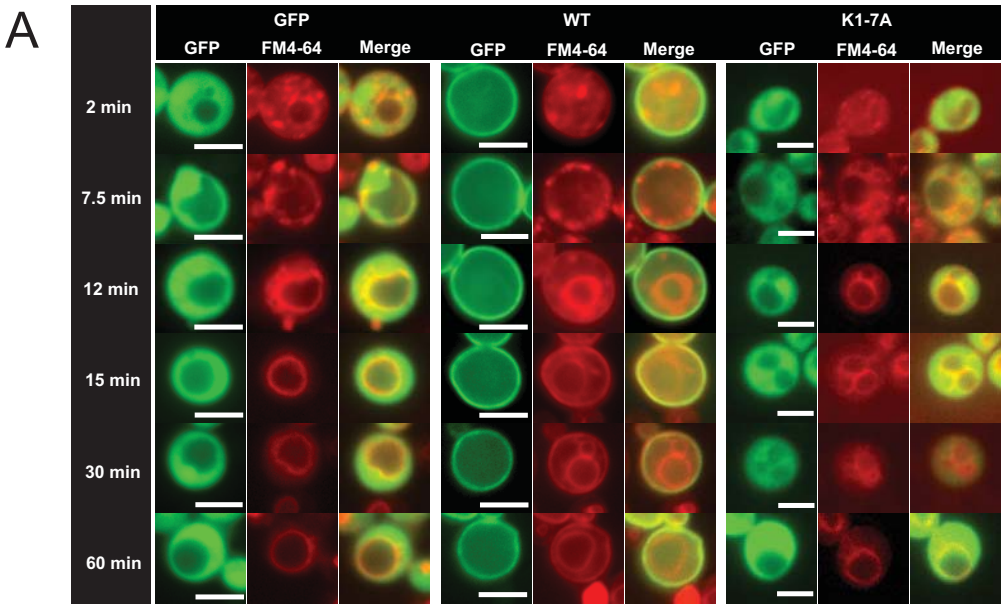

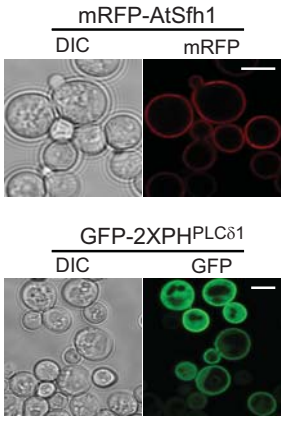

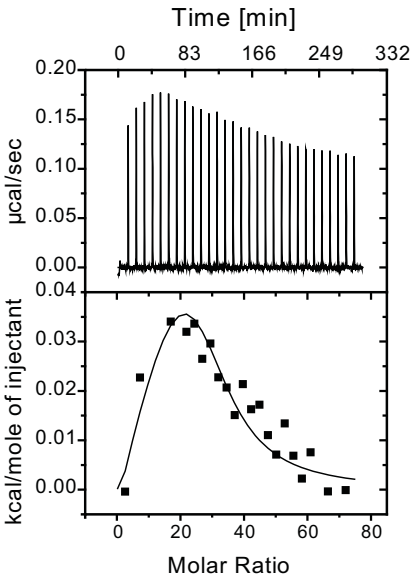

D

	WT	K5A	K35A
N1	0.915 ± 0.2	1.2 ± 0.4	0.9 ± 0.2
K1	5.4 ± 0.03.10^4	2.4 ± 0.15 .10^4	1.7 ± 0.1 .10^4
ΔH1 (cal/mol)	- 1.4 ± 0.05.10^5	- 8.0 ± 2.0 .10^4	- 3.3 ± 0.9 .10^4
N2	27 ± 0	19 ± 2	23.6 ± 14
K2	5.1 ± 0.16 .10^4	2.4 ± 0.5 .10^4	1.6 ± 0.2 .10^4
ΔH2 (cal/mol)	4.7 ± 0.9 .10^3	4.0 ± 1.2 .10^3	3.6 ± 1.5 .10^3

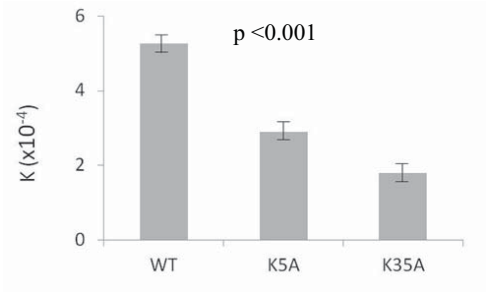

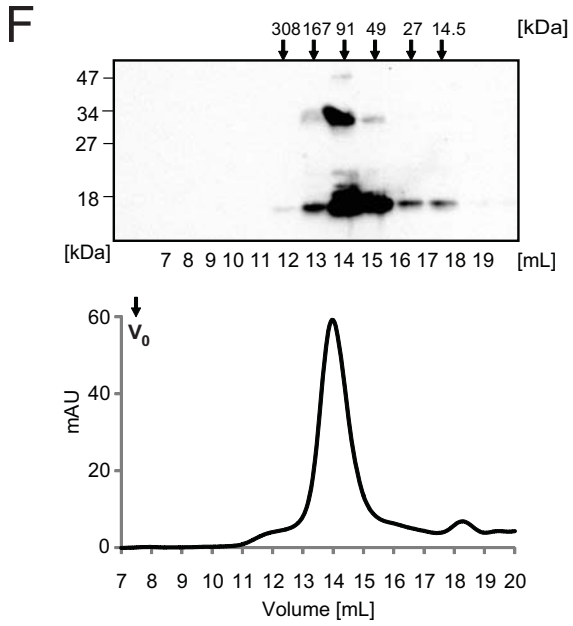

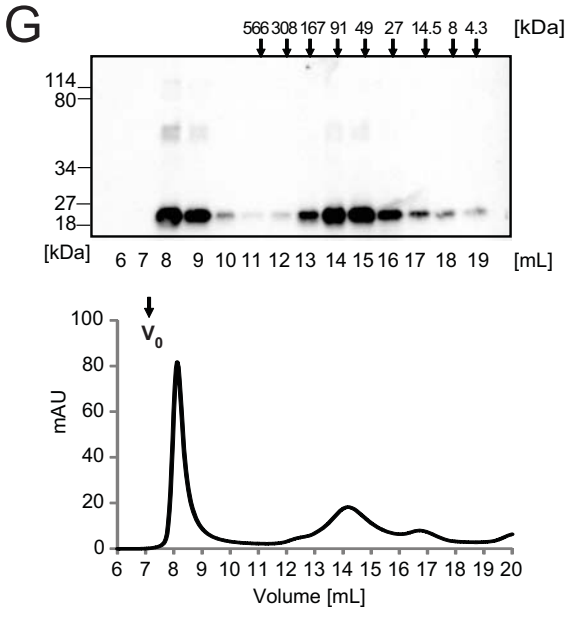

Figure S4

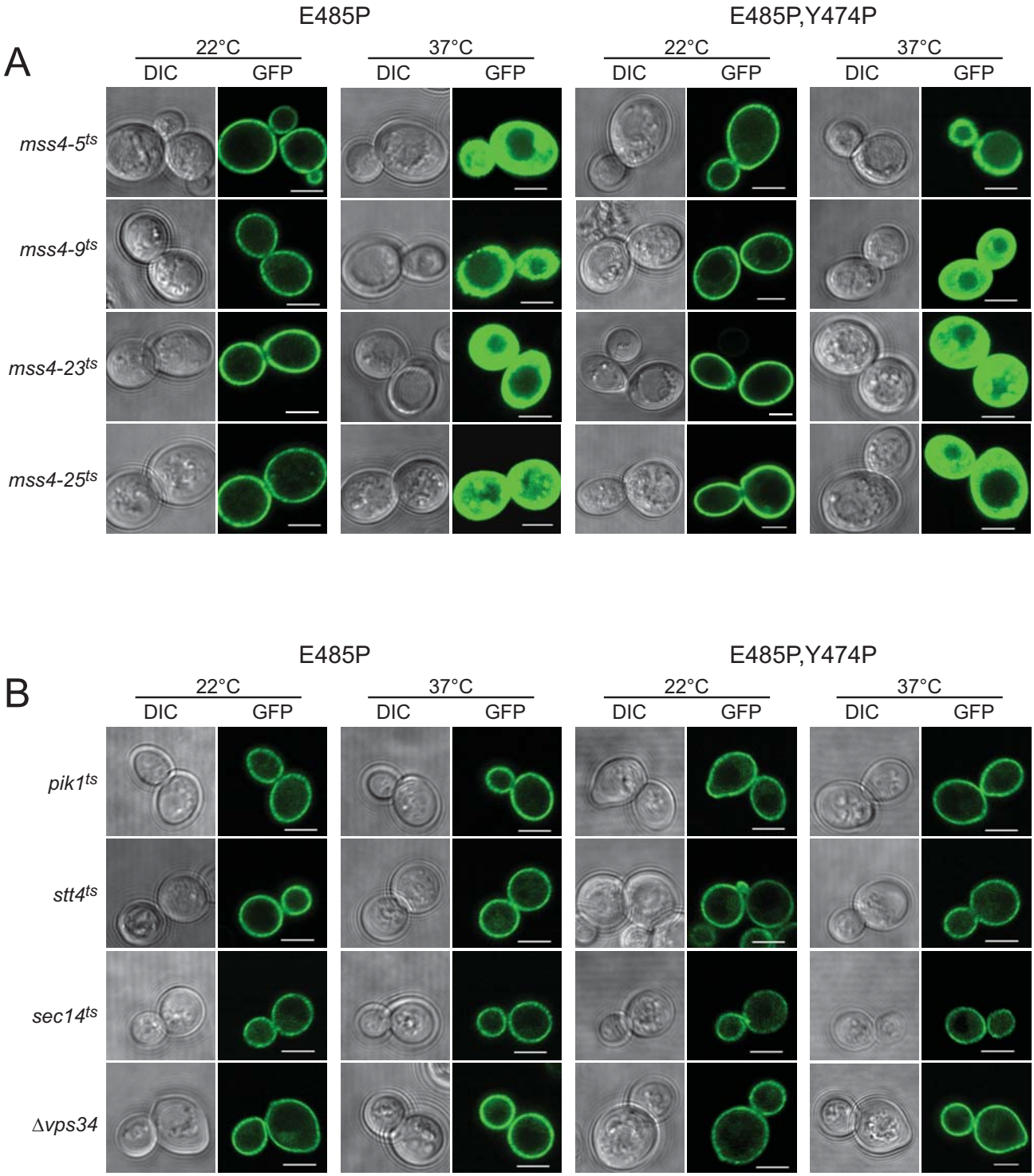
A
E485P
E485P,Y474P
22°C
37°C
22°C
37°C
DIC
GFP
DIC
GFP
DIC
GFP
DIC
GFP
mss4-5ts
mss4-9ts
mss4-23ts
mss4-25ts
B
E485P
E485P,Y474P
22°C
37°C
22°C
37°C
DIC
GFP
DIC
GFP
DIC
GFP
DIC
GFP
pik1ts
stt4ts
sec14ts
Δvps34

Table S1

A

System / number of molecules	AtSfh1	DLPC	DLPS	PIP_2	water	Na^+	Cl^-	Simulation time (microseconds)
1	1	0	0	0	2423	0	7	4
2	1	76	40	12	15439	124	43	1.4
3	2	76	40	12	15328	117	43	1.4
4	4	76	40	12	15184	103	43	1.2
5	2	76	40	12	14842	116	40	1.0
6	8	76	40	12	14354	80	40	1.0

Composition of simulated systems. Peptide in the systems 2-4 was unstructured in the beginning of the simulation, and in the systems 5 and 6 taken from the end (at four microseconds) of the simulation 1.

C

Number of PIP_2 sequestered by the peptide	Average
0	5.91%
1	27.51%
2	34.90%
3	33.18%
4	3.69%

Probability for the number of PIP_2 lipids bound to the peptide during 300-1000 ns.

B

Residue	Group	PIP_2	PS	PC
1LYS	PP(PIP_2)/COO(PS)	0.67	0.20	-
	P	0.02	0	0.16
	OC-Ca	0	0	0
2LYS	PP(PIP_2)/COO(PS)	0.12	0.53	-
	P	0.14	0.12	0.16
	OC-Ca	0	0	0
3LYS	PP(PIP_2)/COO(PS)	0.40	0.10	-
	P	0	0	0.23
	OC-Ca	0	0	0
4LYS	PP(PIP_2)/COO(PS)	0.52	0.35	-
	P	0	0.18	0.17
	OC-Ca	0	0	0
5LYS	PP(PIP_2)/COO(PS)	0.47	0.22	-
	P	0	0.18	0.31
	OC-Ca	0	0	0
6LYS	PP(PIP_2)/COO(PS)	0.40	0.30	-
	P	0	0.25	0.43
	OC-Ca	0	0	0
7LYS	PP(PIP_2)/COO(PS)	0.50	0.22	-
	P	0	0	0.11
	OC-Ca	0	0	0
8LYS	PP(PIP_2)/COO(PS)	0	0	-
	P	0	0	0
	OC-Ca	0	0	0
9PHE	PP(PIP_2)/COO(PS)	0	0	-
	P	0	0	0
	OC-Ca	0	0	0
10PHE	PP(PIP_2)/COO(PS)	0	0	-
	P	0	0	0
	OC-Ca	0	0	0
11GLY	PP(PIP_2)/COO(PS)	0	0	-
	P	0	0	0
	OC-Ca	0	0	0
12PHE	PP(PIP_2)/COO(PS)	0	0	-
	P	0	0	0
	OC-Ca	0	0	0

Average (300-1000 ns from systems 2-6 in Table S1) number of hydrogen bonds formed by peptides with lipids. Here, PP refers to inositol phosphate, P refers to lipids, OC refers to carbonyl group of lipids (see Fig. 4).

D

PtdIns type	Number of hydrogen bonds
PtdIns(4,5)P_2	38.67 (+/- 0.02)
PtdIns(3,5)P_2	27.55 (+/- 0.01)

Average number of hydrogen bonds between 8 peptides and PtdIns present in the system (in 200– 500 ns).

E

Seedling Type	Root hair (RH) size	Double RH% (DRH)	Notch RH%	Triple RH% (TRH)
WT	158.16±115.16	0	0	0
Atsfh1$^{0/0}$	42.48±26.18	37.25	0	0
AtSFH1	153.83±109.39	0	0	0
K_5A	104.3±80.47	9.63	2.52	0.485
K_6A	69.29±56.86	13.88	12.77	0
$K_{3,5}A$	53.89±28.40	48.55	0	0.57
$K_{4,5}A$	38.40±22.32	43.10	0.63	1.07
$K_{3,4,5}A$	28.17±18.19	32.4	0	0.67
$K_{1-7}A$	39.37±25.7	47.83	0	0.49

Root hair lengths (RH), frequencies of double root hairs (DRH), notched root hairs, and triple root hairs (TRH) are given for 3-day old seedlings of wild-type and *Atsfh1*$^{0/0}$ plants (positive and negative parental controls, respectively. The same parameters are given for T_3 *Atsfh1*$^{0/0}$ plants reconstituted for expressing of WT AtSFH1 or mutant Atsfh1 transgenes harboring the indicated C-terminal Lys-Ala (K→A) missense substitution mutations.